SAND2009-8371C

Thermal microactuator performance as a function of mechanical stress

Leslie M. Phinney,* Matthew A. Spletzer, Michael S. Baker, and Justin R. Serrano
Sandia National Laboratories, P.O. Box 5800, Albuquerque, New Mexico, USA 87185

ABSTRACT

We report on the effects of mechanical stress on thermal microactuator performance. Packaging processes such as die attach and lid sealing usually result in stresses on the die containing microsystems devices. While this phenomenon is known, quantifying the effects systematically is difficult due to challenges in controlling the resultant stress resulting from packaging. In this study, we use a four-point bending stage to apply loads of 12 lbf in tension and compression to 11.5 mm by 2.9 mm samples. Thermal microactuators and stress gauges were fabricated using the Sandia 5-layer SUMMiT surface micromaching process and diced to fit in the bending stage. At each stress level, the vernier scales on the thermal microactuator were imaged in order to determine the displacements. Thermal microactuator displacements are reported as a function of applied current up to 35 mA at varying stress levels. Increasing tensile stress decreases the initial displacement and flattens the thermal microactuator displacement versus applied current curve. Raman spectroscopy and stress gauge measurements indicate that the stress range for the four-point bending stage experiments extends from 200 MPa tensile to -250 MPa compressive. Numerical model predictions of thermal microactuator displacement versus current are in qualitative agreement with the experimental results. Quantitative information on the reduction in thermal microactuator performance as a function of stress provides validation data for MEMS models and can guide future designs so that they will be more robust to stresses resulting from packaging processes.

Keywords: Thermal microactuator, mechanical stress effects, MEMS packaging, four-point bending stage

1. INTRODUCTION

Microsystems and microelectromechanical systems (MEMS) have advanced significantly over the last two decades with several devices developing from laboratory prototypes to commercial products. Packaging is one of the most significant challenges in transferring proven microsystems prototypes into applications, often representing a significant fraction of the final product cost as well as not being well understood [1]. Packaging processes for microeletronics and MEMS typically include multiple thermal cycles which result in mechanical stresses on the die and MEMS components when completed [2-3]. These stresses can impact the MEMS performance and reliability. In order to quantify this phenomenon, we initiated an investigation into the effects of mechanical stress on thermal microactuators.

Thermal microactuators are enabling components in many MEMS designs. Advantages of MEMS thermal actuators include higher force generation, lower operating voltages, and less susceptibility to adhesion failures compared to electrostatic microactuators. Thermal microactuators do have higher power requirements than electrostatic microactuators, and their switching speeds are limited by the cooling time. Multiple thermal microactuator designs have been demonstrated, and this study focused on symmetric thermal microactuator designs fabricated from a single material that have been referred to as bent-beam, chevron or V-shaped actuators. Extensive work has been performed designing, fabricating, testing, and modeling this type of MEMS thermal actuator [4-8].

This paper reports on a study of the effects of stress on the performance of MEMS thermal microactuators. In the experimental methods section, we discuss the thermal microactuator and stress gauge design and fabrication, four-point bending stage experimental apparatus and procedures, and measurement of stress using Raman microscopy. The use of the bending stage allowed the stress experienced by the die and MEMS devices to be varied systematically. We present the measured thermal microactuator performance as a function of current at varying loads. Raman spectroscopy and stress gauge measurements were used to confirm the stress levels as a function of bending stage load. A numerical model and predicted thermal microactuator displacement as a function of current and stress are described.

* lmphinn@sandia.gov; phone 1 505 845-8484; fax 1 505 844-6620

2. EXPERIMENTAL METHODS

2.1 Test Structure Design and Fabrication

The thermal microactuators used in this study were fabricated using the Sandia SUMMiT V™ surface micromachined process [9]. The SUMMiT V process [9] consist of four structural layers of polycrystalline silicon (polysilicon) and a layer of polysilicon for the base plane. Between each polysilicon layer is a layer of sacrificial oxide. Connections between the layers of polysilicon are made by removing the sacrificial oxide at the desired connection point. After the final deposition process, the sacrificial oxide layers are removed in an acidic solution. In this paper, poly0 refers to the layer of polysilicon deposited on the substrate and poly1, poly2, poly3, and poly4 refer to the structural layers of polysilicon; poly1 being the closest to the substrate and poly4 being the furthest. The poly1 and poly2 layers are deposited such that they can form a laminate of the two layers which will be referred to as poly12.

A chevron or V-style actuator design utilizes fixed-fixed beams that are fabricated with an offset angle to create an amplified linear motion due to the constrained thermal expansion of the resistively heated actuator beams. The heated beams are made from polysilicon, with an I-beam cross section. The actuator geometry is shown in Figure 1 and the beam cross section in Figure 2. The thermal microactuators have four legs arranged in two pairs. The spacing between two beams in a pair is 2.5 μm, and the two pairs of beams are 58.5 μm apart. The distance from the anchor to the shuttle is 400 μm and the offset is 5 μm. The microactuator legs are fabricated from a laminate of the poly12 and poly3 layers that makes up the I-beam cross section. The distance from the substrate to the bottom of a structure containing poly1 is nominally 2.0 μm.

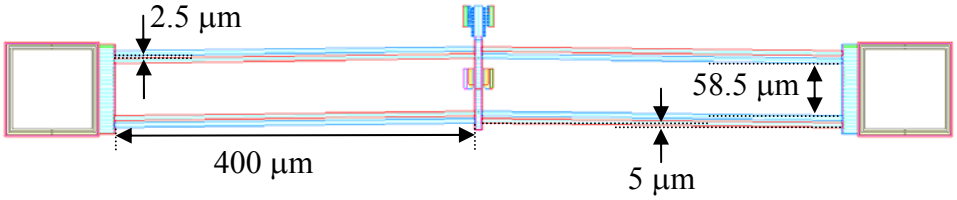

Figure 1. Schematic of thermal microactuator showing the four-legged chevron actuator design.

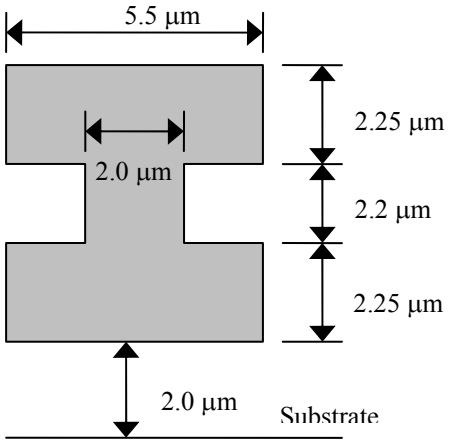

Figure 2. Cross section of a thermal microactuator leg.

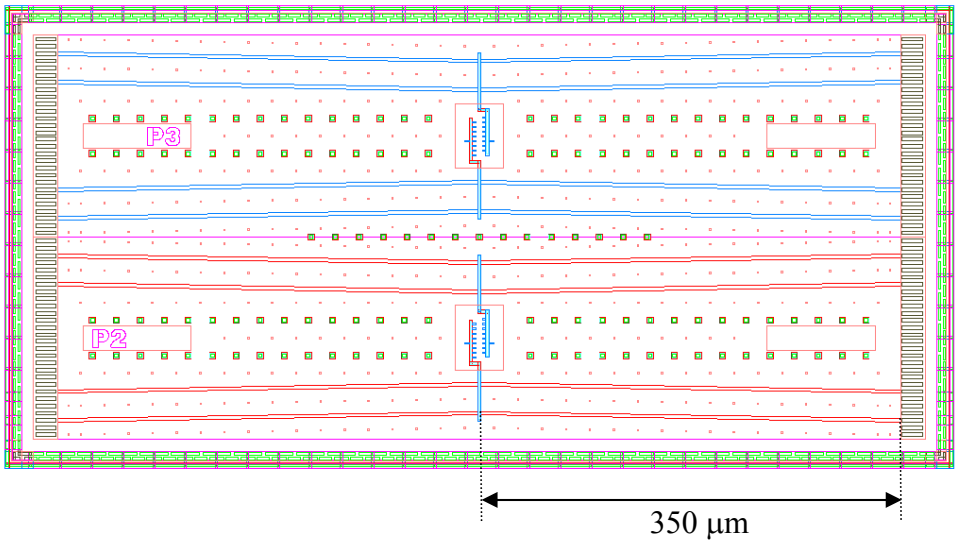

Figure 3. Schematic of the polycrystalline stress gauges. The upper stress is fabricated from the poly3 layer and the lower stress gauge is fabricated from the poly2 layer.

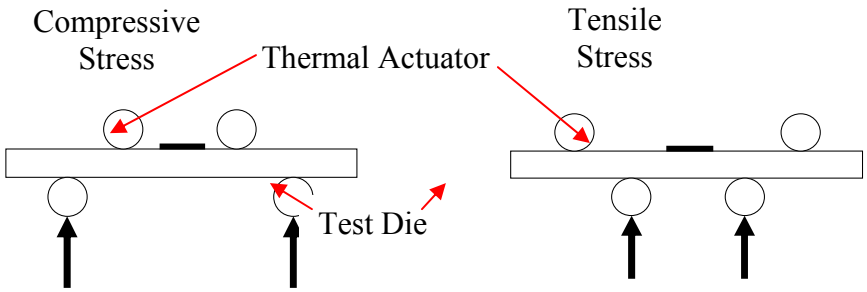

Figure 4. Schematic of the four-point bending stage used to apply either compressive or tensile stress to the die. The arrows indicate the direction of the applied force, and the location of the thermal actuator on the die is indicated..

Two stress gauges were fabricated on the die next to thermal microactuator in order to measure the residual stresses from fabrication processes. Figure 3 shows a schematic of the stress gauges, one of which is fabricated from the poly3 layer and the other from the poly2 layer. The outer markers on the vernier scales of the stress gauges are even indicating a zero stress condition. When subject to tensile stress, the scale on the right moves upward and the scale on the left downward; the reverse occurs when compressive stress is applied.

2.2 Four-Point Bending Stage Experiments

The experiments were performed on individual die that were mounted in a four-point bending stage. Depending on the configuration of the supports, the bending stage could place the top surface of the die in either tension or compression, as shown in Figure 4. The force applied to the die was measured using a load cell in the bending stage and converted to an applied stress value using the following equation [10]:

$$\sigma_{\max} = \pm\left(\frac{3P}{bh^2}\right)\left(\frac{L}{4}\right), \tag{1}$$

where P is the total applied load, b is the width of the die, h is the thickness of the die, and L is the distance between the outer set of rollers shown in Figure 1. In this series of tests, values of 8 mm, 2.9 mm, and 675 μm were used for L, b, and h, respectively. The total load applied to the die was increased in steps of approximately 0.8 lbf until either the die fractured or 12 lbf was reached. When converting the load values from the bending stage to stress from Eq. 1, the value from the bending stage is the total load, P, which is split between the two pins.

Sharpened tungsten probes at the end of micromanipulators were used to make electrical contact with the thermal microactuator bond pads. The optical microscope integrated into a Polytec MSA-400 system was used to view the thermal actuator and assist in aligning the probes on the thermal actuator bond pads. An image of the actuator with the probe tips in place is shown in Figure 5. A Keithley SourceMeter was used to supply a fixed current to the thermal actuator and measure the resulting voltage. The digital camera in the Polytec MSA-400 system was then used to capture an image of the vernier structure on the deflected thermal actuator. Based on guidance from modeling data and past performance, current values of 0-35 mA in 5 mA steps were applied to the actuator. The current was switched off in between each step to ensure the thermal microactuator returned to its original shape and no plastic deformation had occurred. Images of the actuator were captured at each current setpoint before changing applied force levels.

In addition, images of two stress gauge structures located directly adjacent to the thermal microactuator were also captured. These gauges were designed to give a visual indication of the surface stresses in the various layers on the top surface of the die. However, these gauges were designed primarily to measure the residual stress due to fabrication processes and their useful range was only from -75 MPa (compressive) to 10 MPa (tensile); therefore, it was not possible to compare the surface stress readings from the gauges to the values obtained from Equation (1) over the full range of values tested. An image of one of the stress gauges is shown in Figure 6.

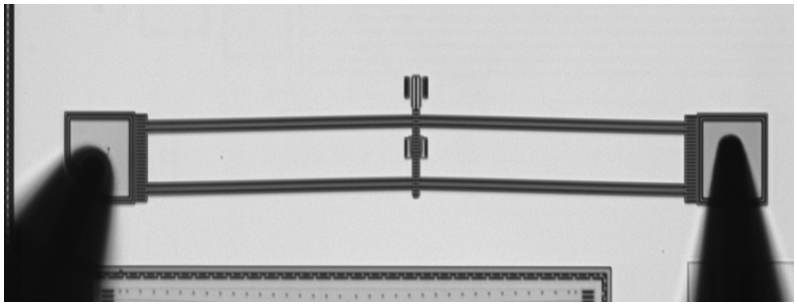

Figure 5. Optical microscope image of a thermal actuator and tungsten probe tips.

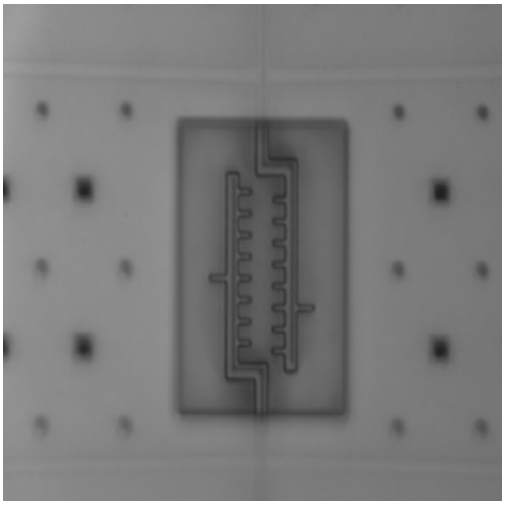

Figure 6. Optical microscope image of one of the stress gauge structures located adjacent to the thermal microactuator indicating a compressive stress since the scale on the right lines up below the scale on the left.

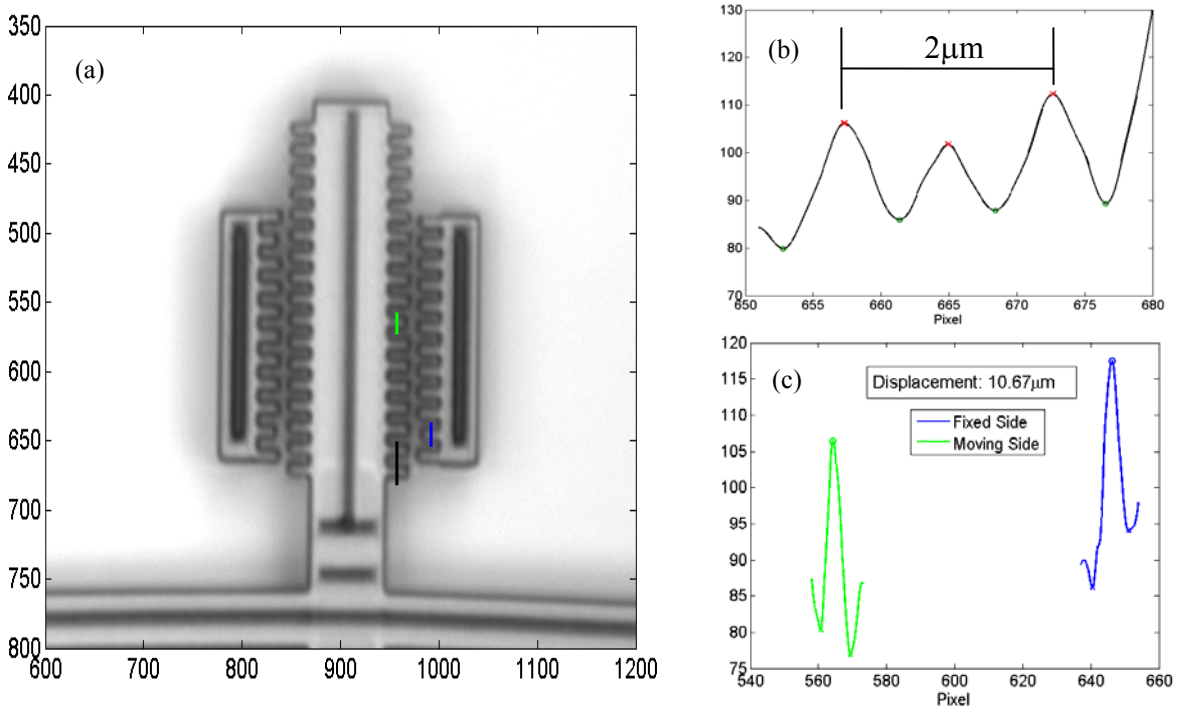

Figure 7. (a) Optical microscope image of the vernier structure on the thermal actuator. The black line indicates the location of the intensity profile shown in (b), and the blue and green lines indicate the location of the shorter tines used to determine the thermal actuator displacement. (b) Intensity profile used to calculate the μm/pixel image scale factor. (c) Intensity profiles used to calculate the displacement of the thermal actuator.

2.3 Image and Data Analysis

Once individual images of the vernier structure on the actuator had been captured at each current value and applied force level, the images were processed using a Matlab script to determine the displacement of the actuator. A scale factor relating distance in pixels to distance in μm was calculated by extracting the intensity profile along a line across two adjacent tines on the thermal actuator, determining the number of pixels between the two tines, and relating that to the known spacing of the tines (nominally 2μm). The displacement of the thermal actuator was then calculated by extracting the intensity profiles across the short tines of the thermal actuator and fixed vernier structure, determining the number of pixels between the peaks in the two intensity profiles, and converting that value to μm using the calculated scale factor. The point at which the two short tines were aligned was considered to be the zero displacement point. Figure 7 shows a representative example of how the scale factor and displacement values were calculated for one particular case.

The stress gauge values were read visually from the microscope images. These values were input into a previously model that was developed during their design to calculate the stress values and standard deviations from the stress in the range of operation, -75MPa to 10 MPa, where compressive stresses are negative and tensile ones positive.

2.4 Stress measurements using microRaman spectroscopy

To determine if there is any difference between the tensile stress experienced by the actuator and the substrate it is necessary to effectively measure stress on both surfaces independently. This was accomplished with microRaman spectroscopy, which has been shown to be an effective tool for mapping stress in microsystems and microelectronics [11-13]. The system used was a Renishaw inVia Raman microscope, with 180° backscattering geometry and a 488 nm Ar+ laser as the probe. The beam is focused to a ~560 nm diameter spot with a 50×, 0.50 numerical aperture (NA)

objective; spreading of the beam within the sample results in a measurement diameter of ~1.5 μm. Raman signal arising from the sample surface is collected through the objective, dispersed by a grating spectrometer with a spectral resolution of 0.95 cm^{-1}/pixel of the collection CCD. The laser power at the sample is attenuated to 100 μW to minimize localized heating of the sample that could otherwise introduce a bias into the measurement.

For the polycrystalline silicon samples studied, the change in the frequency of the Stokes Raman scattered light resulting from the optical phonon mode at the Brillouin zone center is used as the stress metric. At a constant temperature, the position of the resulting Raman peak from the surface is shifted to lower frequencies whenever a tensile stress is applied due to deformation of the interatomic potentials. The relationship between the change in the peak position and change in hydrostatic stress is given by

$$\Delta\omega = A\Delta\sigma_H = A\Delta\left(\frac{\sigma_{xx}+\sigma_{yy}}{2}\right), \tag{2}$$

where $A = -3.6$ cm^{-1}/GPa [11]. For the uniaxial stress condition used in the experiment, the equation above reduces to:

$$\Delta\omega = A'\Delta\sigma_{xx}, \tag{3}$$

where, $A' = A/3 = -1.8$ cm^{-1}/GPa. Note that the measure obtained with Raman is the change in the stress level of the surface due to an applied load.

For the verification measurements, the sample is placed in the four point bending stage under the Raman microscope. The Raman probe beam is focused on the surface, and six Raman spectra are collected from the surface. Measurements are taken from the middle point of a single leg of the actuator in the center of the die and from a poly0 base plane near the actuator under various loading conditions of the bending stage. The Raman signal is collected for 20 s at each load different condition, up to a load of ~11 lbf (corresponding to an estimated tensile stress of 225 MPa). To account for possible drift in the system, Raman data is acquired from a silicon reference sample integrated into the microscope prior to each measurement under load.

3. EXPERIMENTAL RESULTS

3.1 Thermal Microactuator Performance

A total of three die were tested-two in tension, and one in compression. The results of the displacement measurements for the two die tested in tension are shown in Figures 8 and 9.

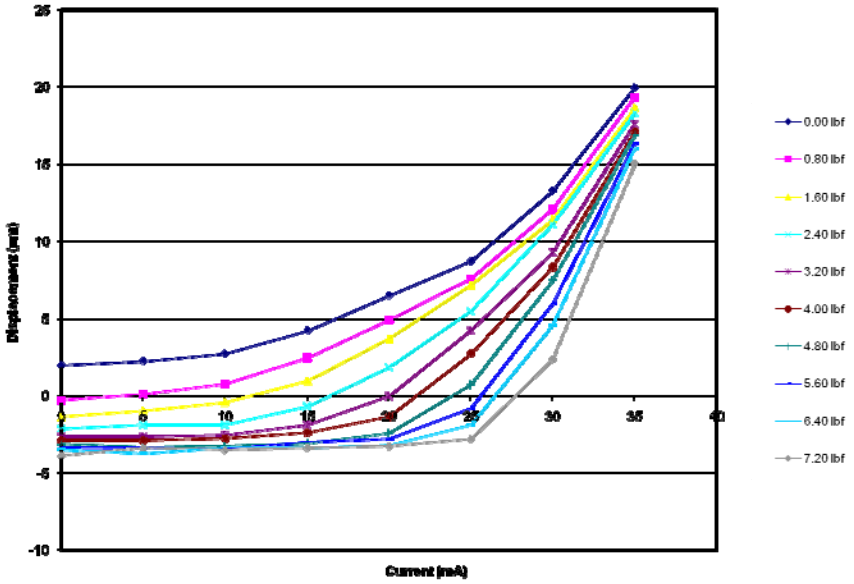

Figure 8. Displacement versus applied current curves for the first thermal microactuator tested in tension. After the 7.20 lbf test, the load was increased to slightly above 12 lbf, and the die fractured.

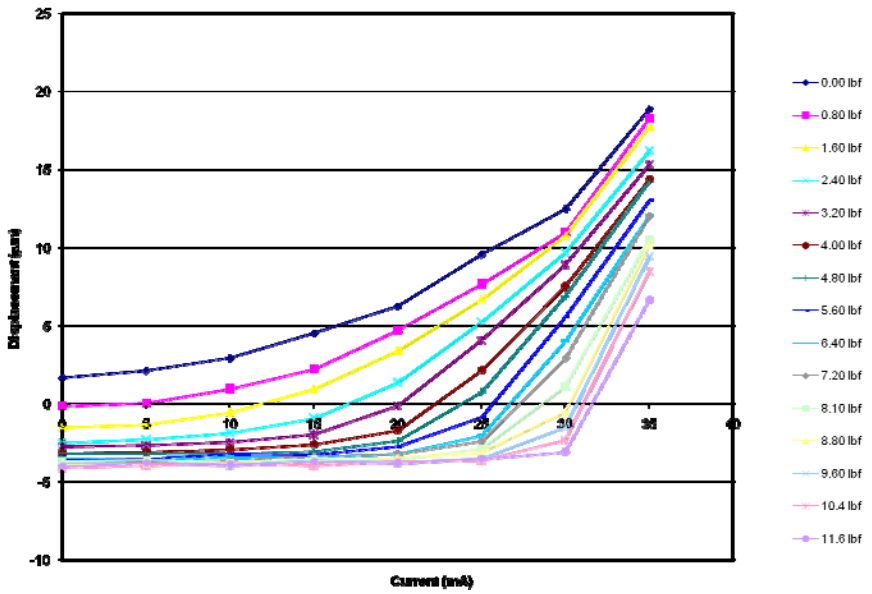

Figure 9. Displacement versus applied current curves for the second thermal microactuator tested in tension. The die fractured when the load was increased above 11.6 lbf.

The initial positive displacement observed at zero applied stress and zero applied current is consistent with the fact that residual compressive stress is present in micromachined structures after the SUMMiT V process. The poly2 and poly3 stress gauges measured the residual stress as -21.72 ± 1.57 MPa and -15.75± 1.47 MPa, respectively, for all three of the thermal microactuators tested, two in tension and one in compression. Both thermal microactuators tested in tension show consistent trends in overall behavior as the applied tensile load is increased. At zero current, the displacement decreases and eventually reaches a minimum of approximately -4 μm. This corresponds to the point at which the thermal actuator has been stretched from its original chevron shape to a nearly flat line; past that point, additional tensile stress results in little shape change in the actuator and therefore little change in initial displacement. At low applied tensile load values, each increase in current results in a measurable change in displacement; however, as the load is increased, higher current values are required to produce displacement change. At the highest load values shown in Figure 9, almost no displacement is observed until 35 mA is applied to the themal microactuator. In addition, over the range of tensile load values tested, the maximum displacement of the actuator decreased by more than 60% as the applied load was increased.

The results of the displacement measurements for the die tested in compression are shown in Figure 10. Once the applied force reached 5.60 lbf, an applied current of 35 mA resulted in the legs of the thermal actuator contacting the fixed portion of the vernier structure; therefore, the current was limited to a maximum of 30 mA at higher force levels. The results of the compression tests are consistent with those of the tension tests: as the compressive load increases, the initial displacement of the actuator increases. In general, at low load values, increasing the applied current results in a measurable deflection change. At higher applied compressive loads, some flattening of the curves does occur at low current values; however, the effect is nowhere near as pronounced as in the tensile stress cases. The presence of the fixed side of the vernier structure prevents a comparison of the maximum deflection reached at an applied current of 35 mA, however, at 30 mA, the displacements consistently increase with increasing compressive load, continuing the trend observed in the tensile data.

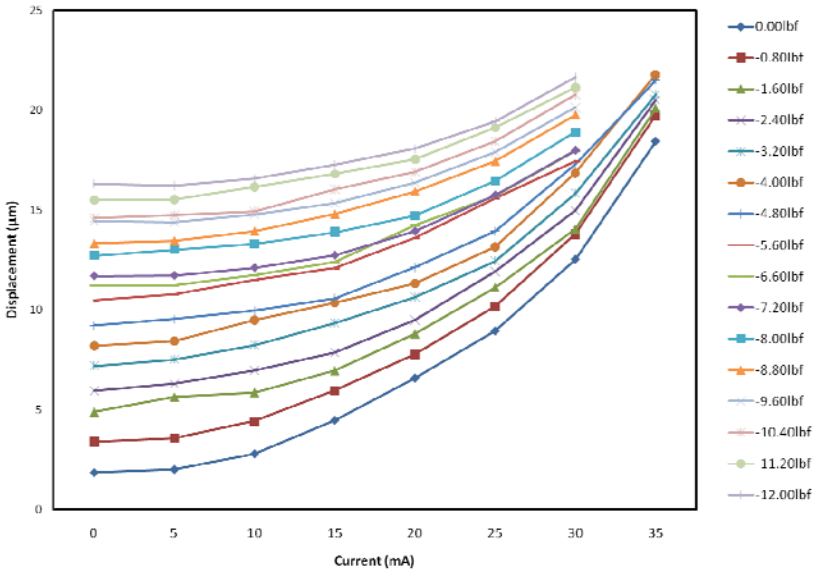

Figure 10. Displacement versus current curves for the die tested in compression.

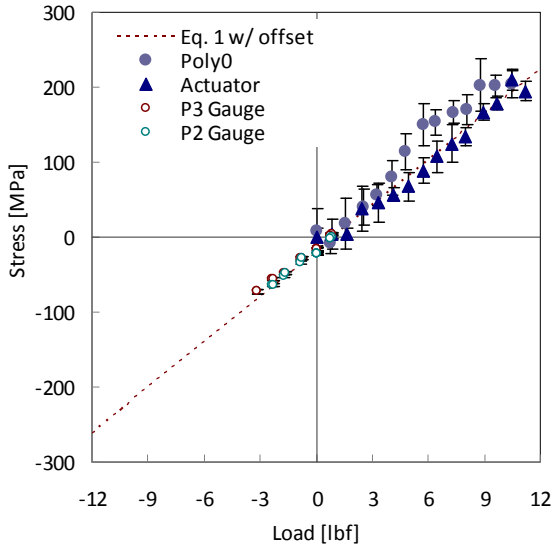

Figure 11. Measured stress change as a function of applied load to the bending stage: solid symbols indicate Raman measurements and open symbols indicate on-die stress gauge measurements. The dashed line indicates the stress calculated with Eq. 1 with a compressive stress offset of -18.735 MPa determined from the gauge measurements under no-load conditions.

3.2 Stress Measurements

After acquiring the Raman data as described in the experimental methods section, the spectra are fitted with a Voight (Gaussian-Lorentian convolution) function and the position of the Raman peak is extracted. The peak position values are then converted into stress using temperatures using Eq. 3. The uncertainty of the measurement, after accounting for system drift, is ~ ±25 MPa. Figure 11 shows the measured stress as a function of applied load to the bending stage compared to the stress predicted by the four-point bending relationship, Eq. 1, with an offset of 18.735 MPa to account for the residual stress. The stress measured using Raman spectroscopy and using the poly2, P2, and poly3, P3, stress gauges are shown. As seen in the figure, within the uncertainty of the measurement, the Poly0 data agrees well with the trend of the predicted value up to a load of ~9 lbf. The actuator measurement, however, is consistently lower than both

the Poly0 and predicted values. This could be due to relaxation, by bending, of the applied stress as the load is increased. Also, the upper pins of the four-point bending stage are in contact with other micromachined structures on the die which may affect the amount of stress transferred to the die.

4. NUMERICAL MODEL

A coupled electro-thermo-mechanical model of this actuator has been developed to predict actuator performance (displacement, temperature and output force) as a function of the geometry and applied current. The model utilizes a finite-difference thermal model to predict the total thermal strain at a given input current, accounting for temperature dependent material properties including thermal conductivity, electrical resistivity and coefficient of thermal expansion. The commercial finite-element analysis software ANSYS is then used to model the structural response for the given thermal strain. This model is described in detail by Baker et al. [4]. For the geometry shown in Figure 1, predicted displacement as a function of both input current and applied external stress is shown in Figure 12.

The numerical model predictions agree qualitatively with the experimental measurements in Figs. 8-10. The initial displacement decreases and the displacement curve flattens with increasing tensile stress. Quantitatively the model underpredicts the thermal microactuator displacement, even when no external stress is applied. The -20 MPa predictions are the appropriate comparison for the experiments without externally applied stresses due to the -18.7 MPa residual stress in the tested devices. The predicted initial displacement of 2 μm at 0 mA applied current agrees well with the measured values for the 0 lbf cases in Figs. 8-10; however, the predicted displacement at 35 mA is 14 μm which is lower than the measured values of 18.4-20.0 μm. The differences between the numerical model and experimental results can be explained by the numerical model underpredicting the heating occurring at a given current or overestimating the thermal microactuator stiffness reducing the displacement. Further efforts are needed to resolve the quantitative differences between the numerical predictions and measured thermal microactuator displacements.

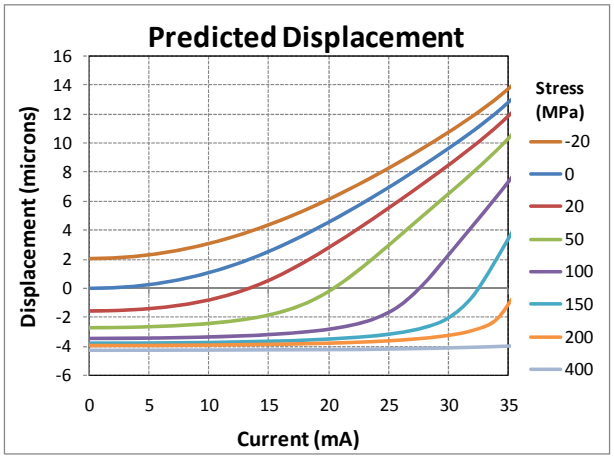

Figure 12. The modeled actuator displacement as a function of both input current and applied external stress.

5. CONCLUSIONS

Packaging processes result in mechanical stresses on microsystems devices that affect their performance and reliability. Due to the challenges in systematically controlling the stresses created during packaging, thermal microactuator performance was investigated at varying stress levels using a four-point bending stage. The bending stage was operated in both tensile and compressive modes applying forces from -12 to 11.6 lbf. Raman spectroscopy and stress gauge measurements of stress indicate that the bending stage applies ±225 MPa of stress. Thermal microactuators were fabricated using the SUMMiT V surface micromachining process, and the microactuator displacement measured at 5 mA increments up to 35 mA at varying stress levels. The residual stress after fabrication was determined to be 18.735 MPa of compressive stress. Increasing the tensile stress on a die containing thermal microactuators decreases the initial displacement and flattens the displacement curve for increasing currents. The maximum displacement of the actuator decreased by more than 60% as the applied tensile load was increased to 11.6 lbf, ~200MPa. Numerical predictions of thermal microactuator displacement agree qualitatively with the experimental measurements but underpredict the displacements quantatively.

ACKNOWLEDGMENTS

Sandia is a multiprogram laboratory operated by Sandia Corporation, a Lockheed Martin Company, for the United States Department of Energy's National Nuclear Security Administration under contract DE-AC04-94AL85000.

REFERENCES

[1] Najafi, K., "Micropackaging Technologies for Integrated Microsystems: Applications to MEMS and MOEMS," Proc. SPIE 4979, 1-19 (2003).

[2] Majcherek, S. and Hirsch, S., "Application of a Method for Characterization of Thermo Mechanical Stress Caused by Packaging Process," Proc. 2nd Electronics Systemintegration Technology Conference, IEEE, 935-940 (2008).

[3] Yang, L., Liao, X.-P., and Song, J., "Effect of Bonding on the Packaged RF MEMS Switch," Proc. ICEPT-HDP 2008, IEEE, 1-4 (2008).

[4] Baker, M. S., Plass, R. A., Headley, T. J. and Walraven, J. A., "Final Report: Compliant Thermo-Mechanical MEMS Actuators LDRD #52553," Sandia report SAND2004-6635, printed December 2004.

[5] Lott, C. D., McLain, T. W., Harb, J. N., and Howell, L. L., "Modeling the Thermal Behavior of a Surface-Micromachined Linear-Displacement Thermomechanical Microactuator," Sensors and Actuators A, 101 (1-2), 239-250 (2002).

[6] Enikov, E. T., Kedar, S. S., and Lazarov, K. V., "Analytical Model for Analysis and Design of V-Shaped Thermal Microactuators," Journal of Microelectromechanical Systems, 14 (4), 788-798 (2005).

[7] Wong, C. C., and Phinney, L. M., "Computational Analysis of Responses of Micro Electro-Thermal Actuators," Proc. 2007 ASME IMECE, IMECE2007-41462, 1-9 (2007).

[8] Kearney, S. P., Phinney, L. M., and Baker, M. S., "Spatially Resolved Temperature Mapping of Electrothermal Actuators by Surface Raman Scattering," Journal of Microelectromechanical Systems, 15 (2), 314-321 (2006).

[9] Sniegowski,l J.J., and de Boer, M.P., "IC-compatible polysilicon surface micromachining," *Annu. Rev. Mater. Sci.*, 30, 299-333 (2000).

[10] Gere, J. M. and Timoshenko, S. P., [Mechanics of Materials, Second Edition], PWS Engineering Publishers, Boston, 205-220 (1984)

[11] Beechem, T., Graham, S., Kearney, S. P., Phinney, L. M., and Serrano, J. R., "Invited Article: Simultaneous Mapping of Temperature and Stress in Microdevices Using Micro-Raman Spectroscopy," Review of Scientific Instruments, 78(6), pp. 061301 (2007).

[12] De Wolf, I., Chen, J., Rasras, M., Spengen, W. M. V., and Simons, V., "High-Resolution Stress and Temperature Measurements in Semiconductor Devices Using Micro-Raman Spectroscopy," Proc. SPIE 3897, 239-252 (1999).

[13] Pomeroy, J. W., Gkotsis, P., Zhu, M., Leighton, G., Kirby, P., and Kuball, M., "Dynamic Operational Stress Measurement of MEMS Using Time-Resolved Raman Spectroscopy," Journal of Microelectromechanical Systems, 17(6), 1315-1321 (2008).